SIMULATION OF THE SYNCHRO-BETATRON SIDEBAND INSTABILITY CAUSED BY ELECTRON CLOUDS AT KEKB

E. Benedetto[1], J.W. Flanagan[2], H.C. Jin[3], K. Ohmi[2],
[1]CERN, Geneva, Switzerland, [2]KEK, Tsukuba, Japan, [3]POSTECH, Pohang, South Korea

Abstract

Electron clouds cause a fast head-tail instability above a threshold density. Experiments at KEKB revealed the presence of a synchro-betatron sideband above the beam blow-up threshold, which indicates the presence of the head-tail instability. The sideband appears near $\nu_y + k\nu_s$, where $1 < k < 2$, which differs from ordinary instability seen near $\nu_y - \nu_s$. We study the origin of the sideband using a computer simulation.

INTRODUCTION

Electron clouds cause a fast head-tail instability due to a two-stream type of interaction between the beam and electron cloud. The instability is observed as an appearance of a synchro-beta sideband above a a certain threshold current of the beam. The sideband appearances at the beam size blowup threshold, as observed by SR interferometer, and its threshold increases as the excitation of cloud-suppression solenoid installed in the KEKB LER is increased. The sideband is a signature of the electron cloud-induced head-tail instability. The sideband appears near the upper side of the betatron tune, $\nu_y + k\nu_s$, where $1 < k < 2$, which differs from the ordinary instability, which is caused by mode coupling between the 0-th mode at ν_y and the -1 mode at $\nu_y - \nu_s$. Both the betatron and sideband tunes are observed in the measurements. This fact indicates that the instability is caused by a coupling of higher synchro-beta modes, for example m=+1 and +2 [1]. Previously, simulations had been performed to reproduce the sideband spectrum, but were not successful [2]. Recently, it has been discovered in simulations that the cloud size strongly affects the sideband spectrum.

SIMULATIONS

The dynamical behavior of a positron beam has been studied with two simulation codes, PEHTS [3] and HEAD-TAIL [4]. The wake field due to electron cloud had been studied by analytical and numerical methods [5]. The cloud size affects the strength of the wake field – i.e., the strength given by the numerical method is consistent with the analytical estimate at a cloud size comparable with the beam size, while it increases 2-3 times for a sufficiently large cloud. The wake field shape strongly depends on the positions of both z and z'.

The simulation gives $\langle y \rangle$, $\langle y^2 \rangle$ and other statistical values of the beam particles turn by turn. Fig. 1 shows the evolution of the vertical beam size, $\sqrt{\langle y^2 \rangle - \langle y \rangle^2}$. There

is no remarkable emittance growth below the density of $\rho_e \leq 6 \times 10^{11}$. An emittance growth appears at 8×10^{11} and become clear at 1×10^{12}. Fig. 2 shows Fourier power spectra of the beam position for the same range of cloud densities. The sideband signal to the right of the betatron peak also appears at 1×10^{12}, and the spacing between the sideband and betatron peaks shifts as the cloud density increases, in agreement with data from machine studies. (Note: the fractional tunes are set $\nu_y = .58$, $\nu_s = .025$; the observed betatron tune peak itself also shifts upwards as the cloud density increases.)
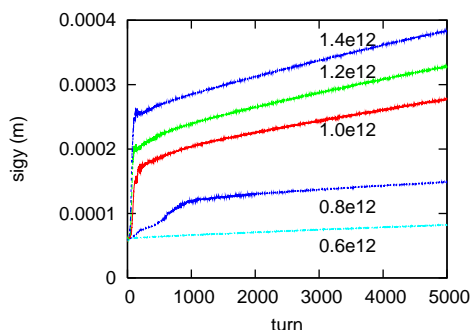
Figure 1: Turn-by-turn beam-size evolution for different cloud densities. (PEHTS)
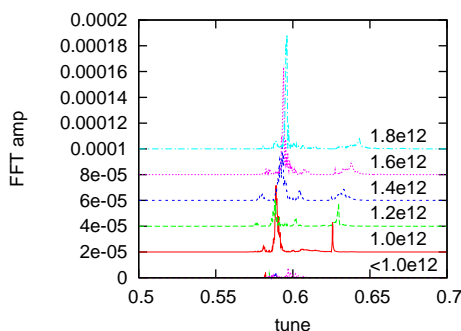
Figure 2: FFT power spectra of beam position data for different cloud densities. (PEHTS)

The Fourier power spectrum of the beam position signal is shown for a range of cloud sizes in Fig. 3. (These data are generated by PEHTS.) The size of the cloud $\sigma_{y,c}$ is expressed in terms of the size of the beam, $\sigma_{y,b} = 60 \ \mu m$. The simulation grid extends $\pm 20 \ \sigma_{y,b}$ for $\sigma_{y,c} \leq 20 \ \sigma_{y,b}$, and $\pm \sigma_{y,c}$ for $\sigma_{y,c} = 30 \ \sigma_{y,b}$ or $40 \ \sigma_{y,b}$. In all cases, the number of grid points was 128×256; the grid spacing for

05 Beam Dynamics and Electromagnetic Fields

D04 Instabilities - Processes, Impedances, Countermeasures

$\sigma_{y,c} = 30\,\sigma_{y,b}$ or $40\,\sigma_{y,b}$ is thus proportionally larger than for $\sigma_{y,c} = 20\,\sigma_{y,b}$.

Previous simulations had been centered around $\sigma_{y,c} = 10\,\sigma_{y,b}$; in that range, as can be seen, there is not such a clear sideband signal. The sideband signal appears clearly to the right of the betatron peak, between $\nu_y + \nu_s$ and $\nu_y + 2\nu_s$, at $\sigma_{y,c} \geq 20\,\sigma_{y,b}$, in agreement with measured data. Note that at $\sigma_{y,c} = 1\,\sigma_{y,b}$, a sideband appears to the left, near $\nu_y - \nu_s$. Data taken from machine studies are more consistent with the simulations of the extended cloud, indicating a wake structure consistent with a cloud of broad extent, $\geq 20\,\sigma_{y,b}$, in the real machine.
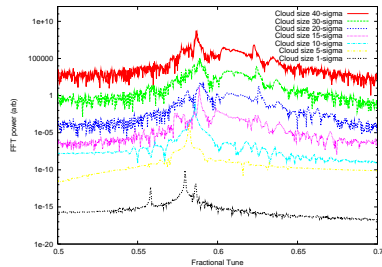
Figure 3: Fourier power spectra of bunch centroid positions for different sizes of electron cloud. Cloud sizes are expressed in terms of the initial size of the beam.

The turn-by-turn evolutions of the vertical bunch sizes at the different cloud sizes are shown in Fig. 4, and the turn-by-turn bunch positions are plotted in Fig. 5. Note that the emittanced growth is very slow for the smallest cloud size, where the ordinary (left-side) head-tail signal appears. For cloud sizes $\geq 20\,\sigma_{y,b}$ the beam size blows up sharply at first and then grows more slowly as the motion of the bunch starts damping out after the first few hundred turns. This is analogous to the burst-like behavior seen in the real machine [1]. The greatest blow-up is actually seen in the intermediate range of cloud sizes, where the dipole motion at ν_y dominates the spectrum.
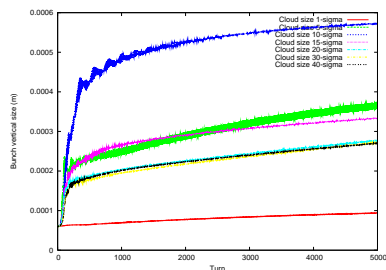
Figure 4: Evolution of vertical bunch size at different sizes of electron cloud. Cloud extents are expressed in terms of the initial size of the beam.

For an idea of what is happening inside the bunches, Figures 6, 7 and 8 show the shapes and sizes of slices along the bunch and cloud for $\sigma_{y,c} = 1\sigma_{y,b}$, $10\sigma_{y,b}$, and $20\sigma_{y,b}$, respectively. Each point in the bunch represents an equal-charge slice of the bunch, and a bunch is sliced into 30
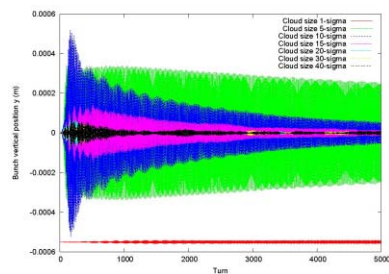
Figure 5: Evolution of vertical bunch centroid position at different sizes of electron cloud. Cloud extents are expressed in terms of the initial beam size of the beam. Note that the 1-sigma cloud data are offset for visibility.

pieces along its length. The simulation gives the *statistical* values of each slice, for all points in the simulation grid, which characterize the inside structure of the bunch and cloud turn by turn. Each figure shows the vertical position and size of the bunch and cloud slices after 100 (top), 300 (middle) and 500 (bottom) turns, for a cloud density of $\rho_e = 1 \times 10^{12}\ m^{-3}$. Clear coherent signals seen the figures are the origin of emittance growth. Note that the cloud has been compressed from its original size by the passage of the bunch. For the case most closely representing the real machine data, the cloud's statistical size remains much larger than that of the bunch, even after pinching, due to the late arrival of electrons from non-linear regions. This seems to be key to the generation of realistic spectra.
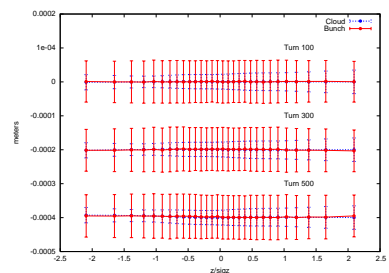
Figure 6: Centroids and statistical sizes of bunch and cloud slices for a cloud size of $1\sigma_{y,b}$. The onset of ordinary head-tail motion can be seen.

The gain of the bunch-by-bunch feedback system at KEKB was not found to have a large effect on the size of the sideband signal. This is also found to be the case in simulation, as seen in Fig. 9, which shows the bunch spectra for a range of feedback gains.

Finally, Figures 10 and 11 show two-dimensional plots of bunch spectrum vs cloud density for RF voltages $V_c = 8\ MV$ and $4\ MV$, respectively. The corresponding synchrotron tunes are $\nu_s = 0.025$ and $\nu_s = 0.0125$. (The momentum compaction factor was adjusted to keep the bunch length and longitudinal emittance constant.) The distance between the betatron tune at 0.58 and the sideband changes at $\rho_e = 2 \times 10^{12}\ m^{-3}$ by the amount of the change in ν_s, in agreement with data [6].

05 Beam Dynamics and Electromagnetic Fields

D04 Instabilities - Processes, Impedances, Countermeasures
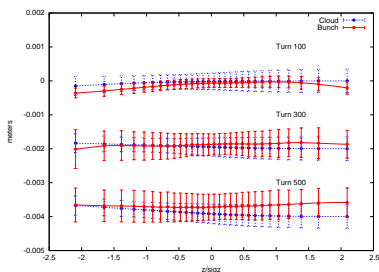
Figure 7: Centroids and statistical sizes of bunch and cloud slices for a cloud size of $10\sigma_{y,b}$. The motion of the bunch is predominantly dipole motion at the betatron frequency, with the maximum amplitude at the center of the bunch.
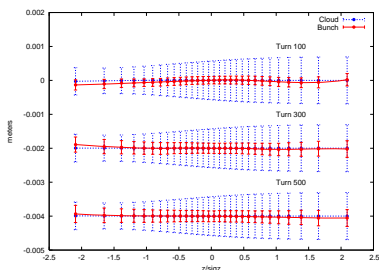
Figure 8: Centroids and statistical sizes of bunch and cloud slices for a cloud size of $20\sigma_{y,b}$. The onset, growth, and start of damping of head-tail motion can be seen. The spectrum of this motion most closely resembles that of real machine data in the presence of electron clouds.
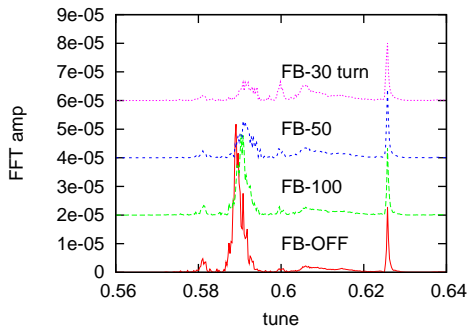
Figure 9: Bunch spectra for varying bunch-by-bunch feedback gains.

Figure 10: Simulation of bunch spectra vs cloud density for RF voltage $V_c = 8\ MV$, $\nu_s = 0.025$. (HEADTAIL)
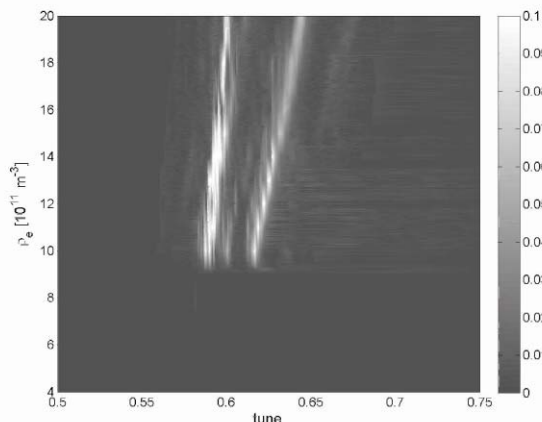
Figure 11: Simulation of bunch spectra vs cloud density for RF voltage $V_c = 4\ MV$, $\nu_s = 0.0125$. (HEADTAIL)

CONCLUSION

The synchro-betatron sideband signal due to electron clouds in the KEKB LER have been reproduced in simulation, agreeing in several quantitative ways with the data observed in machine studies. The dependence of the spacing between the peaks on the synchrotron tune and the cloud density, and the lack of dependence of sideband amplitude on bunch-by-bunch feedback gain are reproduced. In addition, it is found that the cloud size must be $\geq 20\sigma_{y,b}$ to reproduce the observed spectra. Further comparison studies between simulation and data are underway to further understand the detailed mechanism of the instability.

REFERENCES

[1] J. Flanagan et al., Phys. Rev. Lett., 94, 054801 (2005).

[2] K. Ohmi et al., Proc. PAC05, Knoxville, 907 (2005).

[3] K. Ohmi, Proc. PAC01, Chicago, 1895 (2001).

[4] G. Rumolo and F. Zimmermann, "Practical User Guide for HEADTAIL", SL-Note-2002-036 (2002).

[5] K. Ohmi, F. Zimmermann, E. Perevedentsev, Phy. Rev. E65, 165021 (2001).

[6] J.W. Flanagan et al., Proc. EPAC06, Edinburgh, 2898 (2006).

05 Beam Dynamics and Electromagnetic Fields

D04 Instabilities - Processes, Impedances, Countermeasures